

## Microstructure and stopped growth mechanism of Y123 bulk fabricated by directional infiltration and growth

DONG Hao(董昊)<sup>1</sup>, HU Rui(胡锐)<sup>1</sup>, LI Jin-shan(李金山)<sup>1</sup>, KOU Hong-chao(寇宏超)<sup>1</sup>,  
XUE Xiang-yi(薛祥义)<sup>1</sup>, CHANG Hui(常辉)<sup>1</sup>, CAO Hai-tao(曹海涛)<sup>1</sup>, ZHOU Lian(周廉)<sup>1,2</sup>

1. State Key Laboratory of Solidification Processing, Northwestern Polytechnical University,  
Xi'an 710072, China;

2. Northwest Institute for Nonferrous Metal Research, Xi'an 710016, China

Received 1 October 2007; accepted 18 March 2008

**Abstract:** The infiltration-growth process was used as an alternative to conventional melt processing techniques for the preparation of bulk  $\text{YBa}_2\text{Cu}_3\text{O}_{7-x}$  (Y123) with finely dispersed small size  $\text{Y}_2\text{BaCuO}_5$  (Y211) particles. Bulk YBCO superconductors with uniformly distributed particles of micron-sized Y211 were prepared by the directional infiltration and growth (DIG). The microstructure changes of the Y211 particles at various stages of processing were studied. About 70% of Y211 particles are under 1  $\mu\text{m}$  in the final sample. The different stopped growth mechanism of this material along the  $c$  axis and  $ab$  plane was discussed. Undercooling and viscosity lead to tanglesome thick boundary layer. So the Y123 growth along  $c$  axis is stopped. Yttrium lack in front of the  $ab$  plane is the main reason why the growth stops at this direction.

**Key words:** infiltration; superconductor; Y211; YBCO

### 1 Introduction

YBCO bulk high temperature superconductor has significant potential for magnetic levitation device and superconductive permanent magnets due to its high levitation force and high trapped magnetic field [1–2]. The levitation force and trapped magnetic field are proportional to the radius,  $R$ , of the supercurrent loop flowing within the bulk and the critical current density,  $J_c$ , of the superconductor. Now, infiltration and growth (refer to as IG) process has attracted many researchers' attention due to net-shape, homogeneous distribution of fine  $\text{Y}_2\text{BaCuO}_5$  (Y211) and free from crack and pore and so on [3–5]. In conventional melt processing,  $\text{YBa}_2\text{Cu}_3\text{O}_{7-x}$  (Y123) is decomposed to form Y211 phase and Ba- and Cu-rich liquid phase above its peritectic decomposition temperature according to the following equation [6]:



Due to  $\text{O}_2$  releasing, a mass of the macroscopical

and microcosmic defects also appear in the final product and the performance of the bulk is deteriorated. However, in infiltration and growth process, above the peritectic temperature, the barium and copper rich liquid phase infiltrates into Y211 precursor bulk and reacts with Y211 to generate Y123 phase [7–8]. Y123 decomposition is not undergone in this processing. The important advantages of this process are the near net-shape fabrication and the refinement of the Y211 particles with a uniform distribution in the final microstructure [9–11]. Although IG process has evident advantages, it is also difficult to fabricate larger high quality Y123 bulk. So, it is necessary to understand the reason why Y123 domain doesn't always enlarge.

In this work, a directional infiltration-growth (DIG) is adopted to fabricate YBCO bulk superconductors. The microstructure changes of the Y211 particles at various stages of processing are studied. The restrictive factors of Y123 domain growth on the solidification behavior and the microstructures are investigated. The details of stopped growth mechanism of Y123 bulk are discussed.

## 2 Experimental

The precursor Y211 bulk (green) and Ba-Cu-O liquid phase (a mixture of  $\text{Ba}_3\text{Cu}_5\text{O}_x$  and Y123 powders in a molar ratio of 2:1) bulk (black) of 15 mm in diameter were pressed in a mould, respectively. The mass of Y211 bulk was 2.5 g; and the mass of liquid phase was 5.4 g. The Y123 domain was fabricated by directional infiltration-growth. Fig.1 shows the temperature distribution of the furnace along the central axial direction and sketch map of the experimental setup and the sample. Fig.2 shows the time—temperature profile of this process. The equation,  $R_p=v/G$ , was used to connect  $R_p$  with  $v$ . The central axial temperature gradient  $G$  was  $4.3\text{ }^\circ\text{C/mm}$  and the imposed cooling rate  $v$  was  $0.5\text{ }^\circ\text{C/h}$ , so the processing rate  $R_p$  was  $0.12\text{ mm/h}$ . Moreover, the samples were quenched at different stages to study the infiltration and growth of the samples.

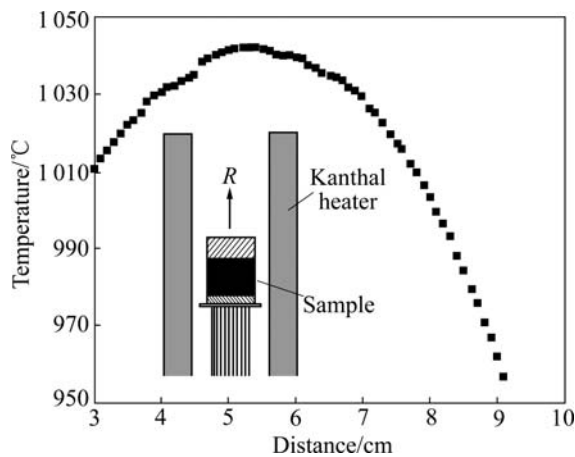


**Fig.1** Temperature distribution of furnace along central axial direction and sketch map of experimental setup and sample

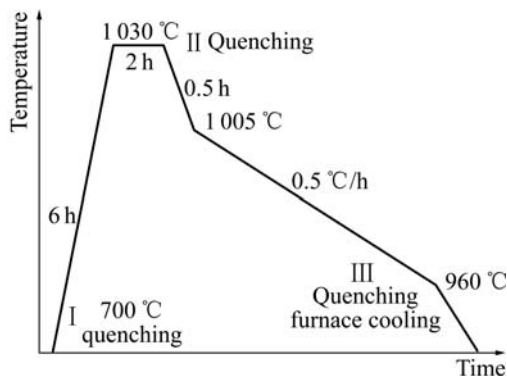


**Fig.2** Time—temperature profile of process used for fabrication of Y123 bulk

The microstructures and morphology of the sample were observed by SEM and OM. The sizes of Y211 powders were analyzed using the laser particle size analyzer. The grain sizes were measured directly from

the micrographs by the Image-Pro Plus 5.0 image processing software. Based on the observation and analysis of the growth front, the phenomenon of the stopped growth was interpreted and some suggestions were provided in maintaining the continuous growth of YBCO grain.

## 3 Results and discussion

### 3.1 Size change of Y211 particles

Fig.3 shows the size distribution of Y211 powders. After prolonging milling by facility and manpower, particles with nearly spherical shape and size distribution ( $0.5\text{--}4\text{ }\mu\text{m}$ ) can be obtained. The average size of particles is about  $1.95\text{ }\mu\text{m}$ . It is believed[12] that the fine Y211 particles will increase the Y123/Y211 interfacial area and induce many micro-defects around Y211 particles, which enhances the flux pinning ability and results in a high  $J_c$  value. So it is important to control the size of the starting Y211 powders for the microstructure of final samples.

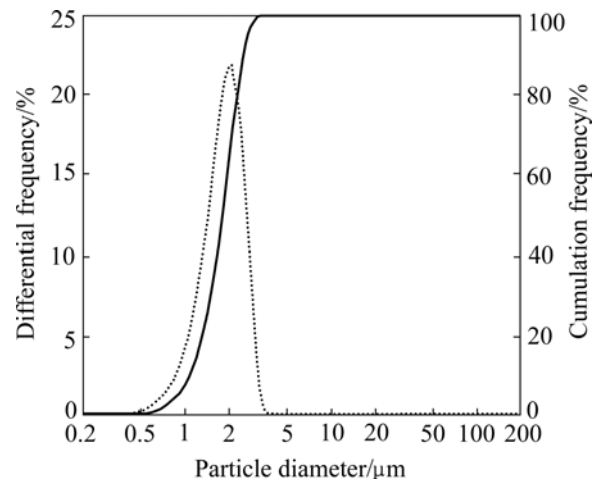


**Fig.3** Size distribution of Y211 powders

Fig.4(a) shows a polished surface of the Y211 precursor bulk corresponding to stage I. At this stage the porosity of the precursor bulk is estimated to be approximately 5% and the Y211 particle morphology is spherical with an average size of  $2\text{ }\mu\text{m}$ . It does not change significantly comparing with the average diameter of starting Y211 powders. Moreover, it can be seen that the liquid phase has infiltrated into Y211 precursor, but it is not even. So Y211 particles should dissolve partially. At the same time, there are also some Y211 particles sintered and this leads to Y211 particles enlarging compared with the starting powders. At stage I, the size of Y211 particles should be redistributed.

Fig.4(b) shows a polished surface of the Y211 precursor bulk corresponding to stage II, i.e. prior to texturing, but after the infiltration of liquid phases. The sample was quenched just after holding for 2 h above  $T_p$ ,

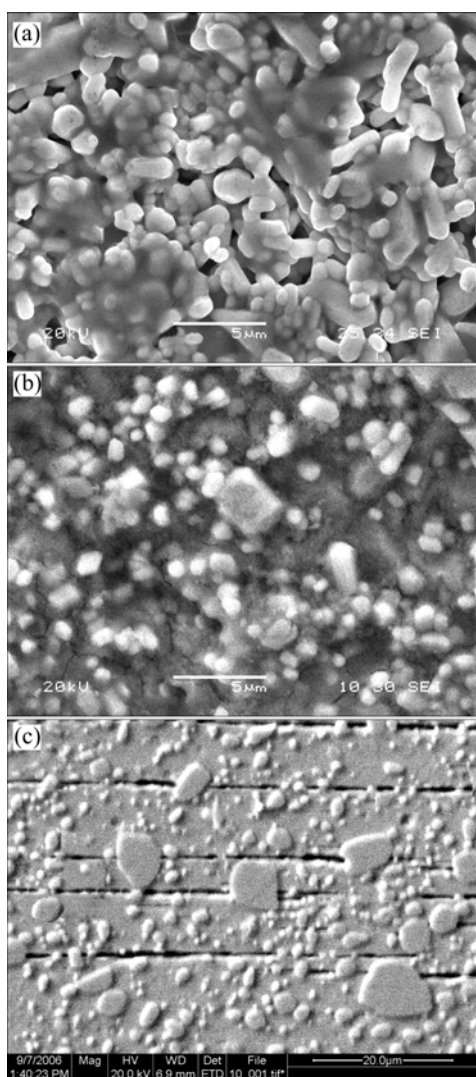


**Fig.4** SEM images of samples at different stages of quenching: (a) Polished surface of sample at stage I ; (b) Stage II ; (c) Stage III

to observe the infiltration of the liquid phases into the Y211 precursor bulk. The white particles are the Y211 phase acted as source of Y-ions by dissolving in the liquid, and the black background is the liquid phase. The SEM image shows that the liquid phases completely fill the vacant regions among the Y211 particles. The size of the Y211 particles in the liquid is smaller than that of the Y211 particles in stage I , but the coarsening of partial Y211 particles in the liquid can also be observed as compared with the particles at the precursor bulk stage I (Fig.4(a)). Since a time of 2 h is allowed for infiltration of the liquid phases and dissolution of Y211 particles above the peritectic temperature, coarsening of Y211 particles has taken place at the expense of dissolution of other smaller Y211 particles in the liquid. Fewer number of Y211 particles at this stage as compared with the stage I supports this view.

Fig.4(c) shows the microstructure of the sample

after texturing stage III . The microstructure reveals oriented domains of Y123 parallel platelets with finely dispersed Y211 particles. The domains like this one range from  $4\text{ mm}\times 3\text{ mm}$  to  $7\text{ mm}\times 5\text{ mm}$  in area. The micrograph also shows a uniform distribution of the Y211 particles. The uniformity of the distribution is an advantage of the process. Also, the sample has less porosity or fewer voids, for the reasons mentioned by BABU et al[13]. In this work, as the cooling rate is  $0.5\text{ }^{\circ}\text{C/h}$  through peritectic temperature, the domain boundaries are clean and free from any liquid phase segregation. This indicates that the liquid phase reacts with Y211 particles completely. In fact, even the cooling rate achieves  $4\text{ }^{\circ}\text{C/h}$  through the peritectic temperature, well Y123 texture microstructure can also be obtained [14]. It is different from the GdBCO, because the higher cooling rate will lead to the segregation of the residual liquid phases to the domain boundaries[15]. This indicates that Y211 particles distribute uniformly and react enough with liquid phase.

Fig.5 shows a comparison of the Y211 particle size in starting powders and in samples at stages I , II and III. From Fig.5 it can be seen that the starting powders are mainly  $1\text{--}3\text{ }\mu\text{m}$  in size. At stage I the particles in size of  $1\text{--}3\text{ }\mu\text{m}$  decrease, and the particles in size of  $0\text{--}1\text{ }\mu\text{m}$  increase gradually. Partial liquid phase infiltrates into Y211 precursor bulk, and the mass of Y211 particles dissolve, so they are refined. At stage II the particles in size of  $0\text{--}1\text{ }\mu\text{m}$  decrease, however the particles in size of  $1\text{--}2\text{ }\mu\text{m}$  increase. Particles dissolve enough owing to the sufficient contact between liquid phase and Y211 particles. At the same time, due to holding for 2 h at  $1\text{ }030\text{ }^{\circ}\text{C}$ , partial Y211 particles enlarge when the liquid phase is saturated in yttrium. At stage III the amount of particles with  $0\text{--}1\text{ }\mu\text{m}$  in size increases and more than 70% of the Y211 particles are less than  $1\text{ }\mu\text{m}$  in size. But the particles in size of  $1\text{--}2\text{ }\mu\text{m}$  decrease and Y211 particles are refined again. According to the Gibbs-Thompson undercooling in which the dissolution of Y211 in the liquid is driven by their radii of curvature[13], smaller size particles dissolve more rapidly. At the same time, the particles in size of  $3\text{--}5\text{ }\mu\text{m}$  increase. This can be explained by Oswald ripening[16]. Oswald ripening appears because the sample is held for a long time at high temperature, as a result partial particles enlarge again.

Fig.6 shows the optical micrograph of the sample at a low magnification after texturing. The uniform distribution of spherical fine Y211 phase (in white) within the Y123 matrix (in gray) can be observed. This is unlike the conventional melt processed materials where the Y211 distribution is not so uniform and Y211 free regions or pools of liquid phases are observed[17]. Due to the Y123 decomposition, the oxygen diffuses out to

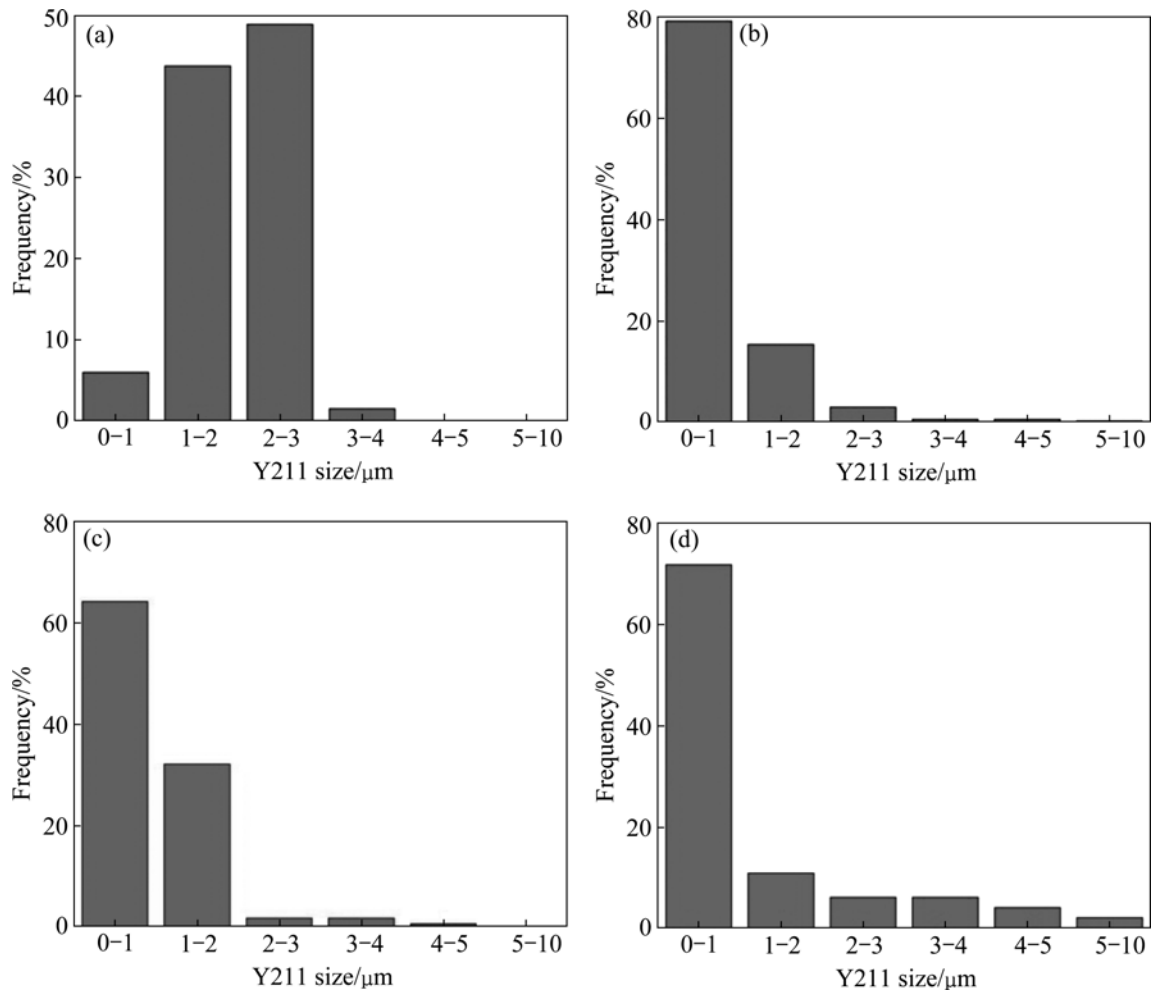


Fig.5 Size distribution of Y211 particles in starting powders (a) and samples at stage I (b), stage II (c) and stage III (d)

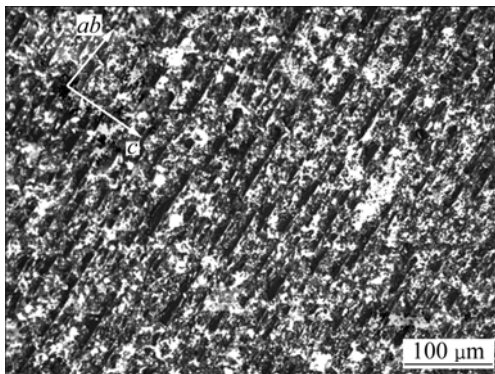


Fig.6 Microstructure of final sample at low magnification

form the pores; they are filled by a liquid phase and spherical liquid pockets containing a few RE211 particles are produced. During the slow cooling in the melt texturing process, the liquid pockets are transformed into the RE123 phases, which do not contain RE211 particles[17]. Since IG process does not involve the decomposition of Y123 within the precursor bulk, a uniform distribution of Y211 particles can be observed at a low magnification (Fig.6).

### 3.2 Stopped growth mechanism of Y123

Although the small domain can be prepared easily, it is difficult to fabricate large and high quality Y123 bulk. In order to fabricate high quality YBCO bulk superconductors with larger size, it is very important to understand the restrictive factors of YBCO bulk growth with excessive Y211.

Fig.7 shows the microstructure at  $c$  axis growth front of Y123 platelets. From this image we can see the evident tanglesome boundary layer with fine Y211 particles between Y123 platelets and liquid phase along  $c$  axis direction. Also, a mass of Y211 phase (in white) with large size can be observed in the liquid phase at the bottom of the boundary layer. So this can be explained by the following reason. Due to the pushing/trapping of Y211 particles and Y211 particles dissolution, the conditions at the interface of Y123/liquid phase, such as undercooling and viscosity, will be changed continuously. However, considering the intrinsic growth kinetics in front of the interface of Y123/liquid, this intrinsic factors can easily be broken off by the exterior conditions. So, the tanglesome thick boundary layer appears. The compo-

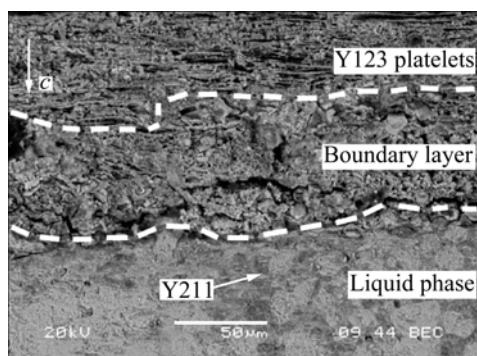


Fig.7 SEM image of boundary layer at  $c$  axis growth direction

sition gradient should be considered as the driving force of the flux. The flux of yttrium ensures the Y123 growth. The decrease of composition gradient with the boundary layer thickness  $\delta$  increasing leads to the decrease of the diffusion rate of yttrium. So the Y123 growth is stopped when  $\delta$  increases to some degree. In this work,  $\delta$  is 60–70  $\mu\text{m}$  when Y123 growth is stopped.

Fig.8(a) shows the microstructure at  $ab$  plane growth front of Y123 platelets and Fig.8(b) shows the polarized optical micrograph with corresponding position to Fig.8(a). From these figures, it can be seen that a clean Y123/liquid phase interface and a clear boundary layer with few Y211 particles are observed. It can be explained that the growth rate in  $ab$  plane is much higher than the diffusion rate of yttrium. So, in front of the  $ab$  plane, yttrium is quickly consumed by the Y123 formation. This leads to yttrium lack. As a consequence, the growth of  $ab$

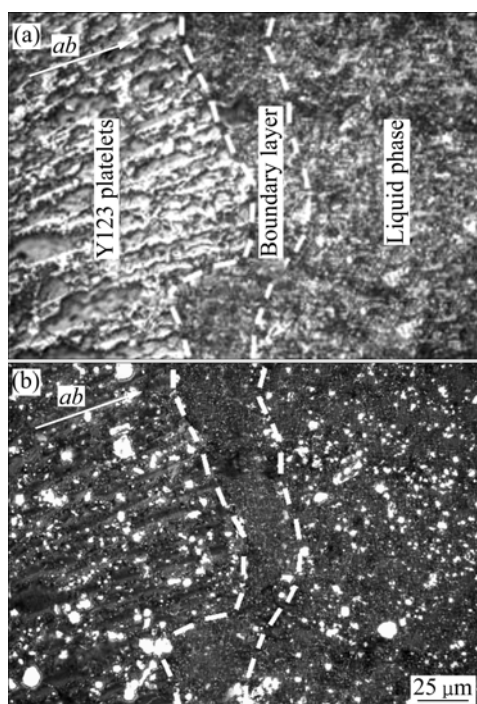


Fig.8 Optical micrograph (a) and polarized optical micrograph (b) along  $ab$  plane at same position

plane stops. The clear boundary layer with few Y211 particles supports this view. The growth front of the  $ab$  plane is not so straight as shown in Fig.8(a). This indicates that the growth front of  $ab$  plane is a complicated curve in microstructure.

The following ways may be able to improve these situations: one is to adjust temperature gradient  $G$  by stages in different direction during Y123 growth to satisfy the intrinsic condition of Y123 growth; another is to reduce the imposed cooling rate  $v$  to be close to the different direction growth rate of Y123. These can result in constant growth and better domain homogeneity.

## 4 Conclusions

1) The comparison of starting Y211 powders and microstructures at different stages of processing reveals that Y211 particles are refined at heating-up stage, and then are coarsened at the heat preservation stages. Y211 particles are refined again after texturing.

2) The resulting samples are highly homogeneous and are free from any liquid phase regions. In the final material more than 70% of the Y211 particles are less than 1  $\mu\text{m}$  in size.

3) Moreover, undercooling and viscosity lead to tanglesome thick boundary layer and the growth along  $c$  axis is stopped when the boundary layer thickness reaches some degree. Yttrium lack in front of the  $ab$  plane is the main reason why the growth stops at this direction.

## Acknowledgement

The authors thank Professor LU Y F and Dr. FENG J Q in the Northwest Institute for Nonferrous Metal Research for their technical supports and helpful discussions.

## References

- [1] MARINEL S, WANG J, MONOT I, DELAMERE M P, PROVOST J, DESGARDIN G. Top-seeding melt texture growth of single-domain superconducting  $\text{YBa}_2\text{Cu}_3\text{O}_{7-\delta}$  pellets [J]. *Supercond Sci Technol*, 1997, 10: 147–155.
- [2] KIM C J, JEE Y A, HONG G W. Variables affecting the fabrication of single grain  $\text{YBa}_2\text{Cu}_3\text{O}_{7-y}$  superconductors by the top-seeded melt growth process [J]. *Supercond Sci Technol*, 2000, 13: 709–715.
- [3] BABU N H, IIDA K, SHI Y, CARDWELL D A. Fabrication of high performance light rare earth based single-grain superconductors in air [J]. *Appl Phys Lett*, 2005, 87: 2025061–2025063.
- [4] NOUDEM J G, MESLIN S, HORVATH D, HARNOIS C, CHATEIGNER D, EVE S, GOMINA M, CHAUD X, MURAKAMI M. Fabrication of textured YBCO bulks with artificial holes [J]. *Physica C*, 2007, 463/465: 301–307.
- [5] IIDA K, BABU N H, SHI Y H, CARDWELL D A, MURAKAMI M. Gd-Ba-Cu-O bulk superconductors fabricated by a seeded infiltration growth technique under reduced oxygen partial pressure [J]. *Supercond Sci Technol*, 2006, 19: 641–647.

- [6] CLOOTS R, KOUTZAROVA T, PMATHIEU J, AUSLOOS M. From RE-211 to RE-123. How to control the final microstructure of superconducting single-domains [J]. *Supercond Sci Technol*, 2005, 18: 9–23.
- [7] MESLIN S, NOUDEM J G. Infiltration and top seeded grown mono-domain  $\text{YBa}_2\text{Cu}_3\text{O}_{7-x}$  bulk superconductor [J]. *Supercond Sci Technol*, 2004, 17: 1324–1328.
- [8] MESLIN S, IIDA K, BABU N H, CARDWELL D A, NOUDEM J G. The effect of Y-211 precursor particle size on the microstructure and properties of Y-Ba-Cu-O bulk superconductors fabricated by seeded infiltration and growth [J]. *Supercond Sci Technol*, 2006, 19: 711–718.
- [9] MATHIEU J P, KOUTZAROVA T, RULMONT A, FAGNARD J F, LAURENT PH, MATTIVI B, VANDERBEMDEN PH, AUSLOOS M, CLOOTS R. Investigation of  $\text{DyBa}_2\text{Cu}_3\text{O}_{7-d}$  superconducting domains grown by the infiltration technique starting with small size Dy-211 particles [J]. *Supercond Sci Technol*, 2005, 18: 136–141.
- [10] IIDA K, BABU N H, SHI Y, CARDWELL D A. Seeded infiltration and growth of large, single domain Y-Ba-Cu-O bulk superconductors with very high critical current densities [J]. *Supercond Sci Technol*, 2005, 18: 1421–1427.
- [11] IIDA K, BABU N H, WITHNELL T D, SHI Y, HAINDL S, WEBER H W, CARDWELL D A. High-performance single grain Y-Ba-Cu-O bulk superconductor fabricated by seeded infiltration and growth [J]. *Physica C*, 2006, 445/448: 77–281.
- [12] ZHOU L, CHEN S K, WANG K G, WU X Z, ZHANG P X, FENG Y. Synthesis of ultrafine  $\text{Y}_2\text{BaCuO}_5$  powder and its incorporation into YBCO bulk by powder melting process [J]. *Physica C*, 2001, 363: 99–106.
- [13] BABU N H, KAMBARA M, SMITH P J, CARDWELL D A, SHI Y. Fabrication of large single-grain Y-Ba-Cu-O through infiltration and seeded growth processing [J]. *J Mater Res*, 2000, 15(6): 1235–1238.
- [14] FANG H, RAVI-CHANDAR K. Fabrication of Y123 disk by the seeded infiltration and growth method [J]. *Physica C*, 2000, 340: 261–268.
- [15] REDDY E S, RAJASEKHARAN T. Microstructural and magnetic properties of textured  $\text{GdBa}_2\text{Cu}_3\text{O}_y/\text{Gd}_2\text{BaCuO}_5$  [J]. *Physica C*, 1999, 316: 279–286.
- [16] ENDO A, CHAUHAN H S, EGI T, SHIOHARA Y. Macrosegregation of  $\text{Y}_2\text{Ba}_1\text{Cu}_1\text{O}_5$  particles in  $\text{Y}_1\text{Ba}_2\text{Cu}_3\text{O}_{7-\delta}$  crystals grown by an undercooling method [J]. *J Mater Res*, 1996, 11: 795–803.
- [17] KIM C J, LEE H G, KIM B B, HONG G W. Origin of  $\text{Y}_2\text{Ba}_1\text{Cu}_1\text{O}_5$  free region in melt-textured Y-Ba-Cu-O oxides [J]. *J Mater Res*, 1995, 10(9): 2235–2240.

(Edited by YUAN Sai-qian)